PNAS Nexus, 2024, 3, pgae216
https://doi.org/10.1093/pnasnexus/pgae216
Advance access publication 5 June 2024
Research Report

Plasmalogen oxidation induces the generation of excited molecules and electrophilic lipid species

Rodrigo L. Faria[a], Fernanda M. Prado[a], Helena C. Junqueira[a], Karen C. Fabiano[a], Larissa R. Diniz[a], Mauricio S. Baptista[a], Paolo Di Mascio[a] and Sayuri Miyamoto[a,*]

[a]Departamento de Bioquímica, Instituto de Química, Universidade de São Paulo, Av. Prof. Lineu Prestes, 748, São Paulo, SP 05508-000, Brazil
*To whom correspondence should be addressed: Email: miyamoto@iq.usp.br
Edited By: Adelia Bovell-Benjamin

Abstract

Plasmalogens are glycerophospholipids with a vinyl ether linkage at the sn-1 position of the glycerol backbone. Despite being suggested as antioxidants due to the high reactivity of their vinyl ether groups with reactive oxygen species, our study reveals the generation of subsequent reactive oxygen and electrophilic lipid species from oxidized plasmalogen intermediates. By conducting a comprehensive analysis of the oxidation products by liquid chromatography coupled to high-resolution mass spectrometry (LC–HRMS), we demonstrate that singlet molecular oxygen [O_2 ($^1\Delta_g$)] reacts with the vinyl ether bond, producing hydroperoxyacetal as a major primary product (97%) together with minor quantities of dioxetane (3%). Furthermore, we show that these primary oxidized intermediates are capable of further generating reactive species including excited triplet carbonyls and O_2 ($^1\Delta_g$) as well as electrophilic phospholipid and fatty aldehyde species as secondary reaction products. The generation of excited triplet carbonyls from dioxetane thermal decomposition was confirmed by light emission measurements in the visible region using dibromoanthracene as a triplet enhancer. Moreover, O_2 ($^1\Delta_g$) generation from dioxetane and hydroperoxyacetal was evidenced by detection of near-infrared light emission at 1,270 nm and chemical trapping experiments. Additionally, we have thoroughly characterized alpha–beta unsaturated phospholipid and fatty aldehydes by LC–HRMS analysis using two probes that specifically react with aldehydes and alpha–beta unsaturated carbonyls. Overall, our findings demonstrate the generation of excited molecules and electrophilic lipid species from oxidized plasmalogen species unveiling the potential prooxidant nature of plasmalogen-oxidized products.

Keywords: plasmalogen, singlet molecular oxygen, hydroperoxides, reactive oxygen species, fatty aldehydes

Significance Statement

Plasmalogens, the most abundant subclass of ether lipids in mammalian cells, have traditionally been regarded as antioxidants. However, our study reveals a new perspective, shedding light on the generation of chemiexcited and reactive lipid species during plasmalogen photooxidation. For the first time, we provide direct evidence revealing the production of excited triplet carbonyls and singlet molecular oxygen as secondary reactive products originating from plasmalogen dioxetane and hydroperoxyacetal intermediates. Importantly, we also demonstrate the generation of electrophilic alpha–beta unsaturated phospholipids and fatty aldehydes through plasmalogen oxidation. These findings highlight the production of excited states and reactive lipid species resulting from plasmalogen oxidation, which can potentially induce oxidative modifications in biological systems.

Introduction

Constituting approximately 15–20% of the total phospholipid pool in mammals, plasmalogens are major structural membrane components crucial for membrane integrity and serving as a reservoir for lipid mediators (1–4). They are the most abundant ether lipids found in all human tissues, especially in the brain and heart (1, 3, 5). While present in anaerobic bacteria, they are absent in plants, fungi, and most aerobic bacteria (5). Plasmalogens possess a vinyl ether bond at the sn-1 position of the glycerol backbone, instead of the typical ester linkage found in other phospholipids. This structural difference confers distinct properties to plasmalogens that profoundly influence membrane organization. Specifically, the absence of carbonyl oxygen at the sn-1 position in plasmalogens promotes stronger inter-molecular hydrogen bonding between the head groups of neighboring lipids that facilitates tighter alignment and packing of phospholipids in membranes contributing to the stability of membrane raft domains and facilitating the formation of nonlamellar structures, such as inverted hexagonal phases (6). These dynamic structures play crucial roles in various cellular processes, including membrane fusion events essential for viral infection and neurotransmitter release. Notably, defects in plasmalogen biosynthesis have been linked to severe neurological pathologies, including Zellweger syndrome (7) and rhizomelic chondrodysplasia punctata (1, 8). Cultured cells and animals

Competing Interest: The authors declare no competing interests.
Received: February 19, 2024. **Accepted:** May 24, 2024

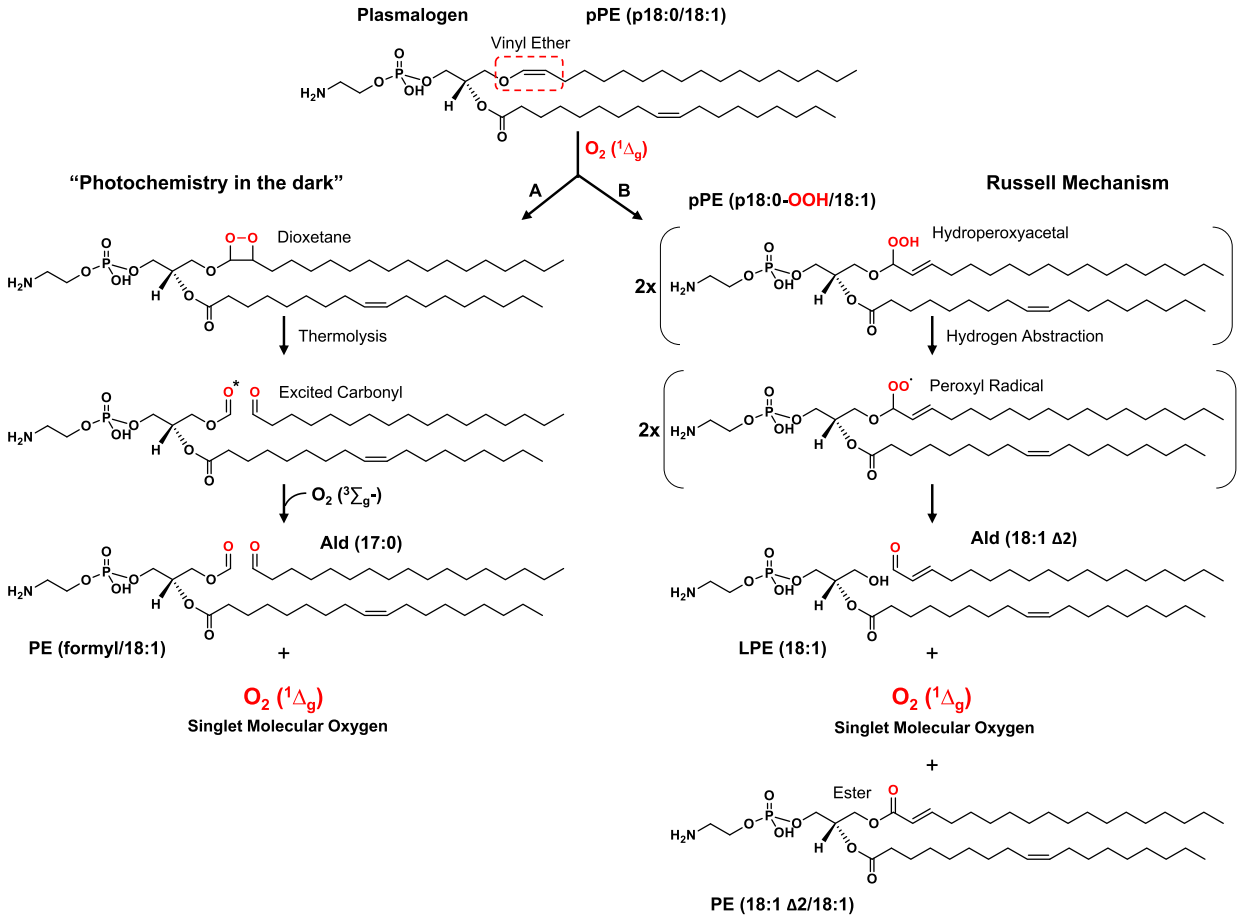

Fig. 1. Scheme depicting the oxidation of phosphatidylethanolamine plasmalogen (pPE) vinyl ether bond by singlet oxygen. pPE (p18:0/18:1) undergoes reaction with O_2 ($^1\Delta_g$), resulting in the formation of dioxetane and hydroperoxyacetal intermediates. A) Thermal decomposition of 1,2-dioxetane generates carbonyl compounds, including one in a triplet excited state (*). These high-energy excited triplet carbonyls can transfer energy to molecular oxygen, leading to the production of O_2 ($^1\Delta_g$). Subsequent C–C bond rupture yields a formyl PE and a fatty aldehyde. B) Decomposition of hydroperoxyacetal results in the formation of peroxyl radicals, either through H atom transfer or metal catalysis. These peroxyl radicals then react, producing O_2 ($^1\Delta_g$), diacyl PE, LPE, and an alpha–beta unsaturated fatty aldehyde.

deficient in plasmalogens have shown to exhibit heightened sensitivity to oxidative damage when compared with their wild-type counterparts (9, 10). Thus, in addition to structural roles, early investigations proposed that plasmalogens act as sacrificial antioxidants due to the high reactivity of their vinyl ether groups with reactive oxygen species, thereby shielding adjacent PUFA from oxidation (10–13). However, recent findings have challenged this notion by revealing a prooxidant and proferroptotic role for ether phospholipids (14–17). For example, elevated plasmalogen levels in cardiomyocytes and neurons have been found to enhance their susceptibility to ferroptosis (15). Nevertheless, the mechanism through which plasmalogens influence cell sensitivity to lipid oxidation remains elusive.

Singlet molecular oxygen [O_2 ($^1\Delta_g$)] is of great importance in chemical and biological systems due to its high reactivity and involvement in physiological and pathological processes (18). Additionally, it serves as tumoricidal and antibacterial components in photodynamic therapy (19). O_2 ($^1\Delta_g$) is generated by light-dependent photosensitized reactions and light-independent chemical and biochemical reactions (20, 21). Singlet oxygen exhibits substantial reactivity toward electron-rich biological molecules, including DNA, proteins, and lipids (20). Among membrane components, plasmalogen vinyl ether bond is highly vulnerable to singlet oxygen–mediated oxidation. The rate constants for both physical and chemical quenching of O_2 ($^1\Delta_g$) by vinyl ether groups have been estimated to be in the range of 10^6–10^7 $M^{-1}s^{-1}$ (22). This is notably 1–2 orders of magnitude faster compared to the reaction with diacyl-phospholipid analogs, indicating that plasmalogens are among the primary targets for O_2 ($^1\Delta_g$) oxidation in biological membranes. However, a comprehensive characterization of primary and secondary oxidation products of plasmalogens is still lacking.

Previous studies have described the generation of dioxetane and hydroperoxide intermediates in plasmalogen oxidation (9, 12, 23). Based on the chemical reactivity of these intermediates, we hypothesized that these intermediates can act as prooxidant species by generating excited molecules and free radicals. For example, the thermolysis of dioxetane produces highly reactive excited triplet carbonyl species (20, 24), which subsequently decay to the ground-state emitting light in the visible region or transfer energy to molecular oxygen, resulting in the production of O_2 ($^1\Delta_g$) (24, 25) (Fig. 1). Notably, the production of chemiexcited species has attracted attention in recent years due to its implications in skin cancer and eye diseases (26–28). Additionally, lipid hydroperoxides can react with metal ions, heme proteins, or other oxidants, producing alkoxyl and peroxyl radicals (29). These radicals can further propagate lipid peroxidation by fueling radical chain reactions and promoting the generation of excited species, such as O_2 ($^1\Delta_g$) (30–34).

In this study, our aim was to thoroughly investigate the formation of reactive species resulting from plasmalogen oxidation with O_2 ($^1\Delta_g$). By utilizing chemiluminescence and liquid chromatography coupled to high-resolution mass spectrometry (LC-HRMS) analysis to characterize primary and secondary oxidation products, we demonstrate the generation of prooxidant and electrophilic lipid species. Our finding reveals that the plasmalogen vinyl ether bond reacts with O_2 ($^1\Delta_g$), leading to the generation of hydroperoxyacetal at the sn-1 position as the major primary oxidation product. Furthermore, we provide evidence for the generation of excited species through chemiluminescence and chemical trapping analysis. Additionally, we developed a specific LC–HRMS method to characterize the production of electrophilic lipid species, including alpha–beta unsaturated phospholipids and long-chain fatty aldehydes. Together, our study highlights the generation of oxidizing excited molecules and reactive lipid species from plasmalogens.

Results

Characterization of plasmalogen photooxidation products

To characterize plasmalogen photooxidation products, a sample of phosphatidylethanolamine plasmalogen (pPE) (p18:0/18:1), was photooxidized at low temperature (−40°C) in the presence of methylene blue (MB). This procedure aimed to prevent dioxetane decomposition. Aliquots of the sample were collected at various time points, and the oxidation products were analyzed by LC–HRMS. During photooxidation, the pPE (p18:0/18:1) peak at 10.3 min was rapidly consumed, nearly depleting after 30 min. Notably, plasmalogen consumption was accompanied by the appearance of a major peak with higher polarity at 9.6 min, along with some minor polar products eluting at earlier retention times, e.g. 4.3 min (Fig. 2A). The photooxidation products were identified through MS (Fig. 2B) and MS/MS analysis (Fig. 2C–F). As expected, pPE (p18:0/18:1) exhibited the deprotonated ion $[M–H]^-$ at m/z 728.5601 (Fig. 2B) and typical fragment ions corresponding to the phosphoethanolamine head group (m/z 140.0118), the 18:1 acyl chain (m/z 281.2486), and two additional fragments resulting from 18:1 acyl chain loss as an acid (m/z 446.3023) or a ketene (m/z 464.3146) (Fig. 2C).

The major product detected at 9.6 min exhibited an m/z value at 760.5483 consistent with the addition of two oxygen atoms to the vinyl ether bond. This product was identified as pPE (p18:0-OOH/18:1), a plasmalogen containing hydroperoxyacetal group at sn-1 position. The MS/MS spectra of this product revealed a prominent fragment ion at m/z 281.2486, originating from both the dissociation of the sn-2-18:1 acyl chain and the dissociation and dehydration (−18) of the sn-1 hydroperoxide alkyl chain (Fig. 2D). Furthermore, to confirm the identity of hydroperoxyacetal group we used triphenylphosphine (TPP) as a reducing agent. Hydroperoxyacetal reduction is expected to produce a hemiacetal intermediate that is cleaved yielding lysophosphatidylethanolamine [LPE (18:1)] and an alpha–beta unsaturated fatty aldehyde [Ald (18:1 Δ2)] (Fig. 2G). Indeed, TPP reduction led to a huge increase in LPE (18:1), confirming the hydroperoxyacetal group (Fig. 2H and Fig. S3). Of note, pPE hydroxide was not detected, thus excluding the possibility of a hydroxide group being formed in the 18:1 acyl chain. Besides the plasmalogen hydroperoxyacetal peak at 9.6 min, two minor polar products eluting at around 4.3 min were identified as LPE (18:1) and formyl phosphatidylethanolamine (PE) (formyl/18:1). These products had similar MS/MS spectra showing major fragments at m/z 281.247 and 140.012 corresponding to the 18:1 acyl chain and phosphoethanolamine. However, PE (formyl/18:1) MS spectra showed a mass shift of +27.99 Da due to the formyl group (Fig. 2E and F).

To further investigate the formation of plasmalogen sn-1 hydroperoxyacetal in a more complex sample, a plasmalogen sample purified from bovine brain was photooxidized under the same reaction conditions (Fig. S1). Interestingly, all plasmalogen species were rapidly consumed within 30 min of reaction, yielding the corresponding hydroperoxyacetal products (Table S1). The formation hydroperoxide at the vinyl ether bond in plasmalogen was confirmed by the MS/MS analysis. All MS spectra showed the characteristic sn-2 fatty acyl chain fragment ions and the sn-1 alkyl chain containing the hydroperoxyacetal group, which showed a mass shift of −18 due to the dehydration of the hydroperoxide group (Fig. S2). Furthermore, reduction with TPP resulted in hydroperoxide consumption, leading to a huge increase in the corresponding LPE products (Table S1). Thus, these data demonstrate that plasmalogen oxidation by O_2 ($^1\Delta_g$) generates hydroperoxyacetal as major primary products.

Determination of the ratio between plasmalogen photooxidation routes

The reaction of singlet oxygen with the plasmalogen vinyl ether group can proceed through two pathways (Fig. 1). The first pathway involves a [2 + 2] cycloaddition reaction mechanism, leading to the formation of 1,2-dioxetanes, and the second pathway involves an *ene* reaction mechanism, resulting in hydroperoxides. Dioxetanes thermally degrade, giving rise to formyl PE and fatty aldehydes (Route A), while ether hydroperoxides can be converted to a hemiacetal intermediate, which spontaneously cleaves, producing LPE and fatty aldehydes (Route B).

To get deeper insights into the mechanism of plasmalogen oxidation via singlet oxygen reaction, we determined the relative amounts of oxidized phospholipid products and long-chain aldehydes arising from both pathways by LC–HRMS analysis. Among the oxidized phospholipid products, PE (formyl/18:1) and pPE (p18:0-OOH/18:1) were used as markers for dioxetane and hydroperoxide pathways, respectively. Notably, plasmalogen hydroperoxyacetal was detected as a major product at all time points of plasmalogen photooxidation (Fig. 3B). The hydroperoxide-to-dioxetane ratio estimated by this approach was 98:2. This ratio was further corroborated by the quantification of long-chain fatty aldehydes, Ald (17:0) and Ald (18:1Δ2), generated from dioxetane and hydroperoxide, respectively (Fig. 3A). Both fatty aldehydes were detected at very low levels in photooxidized samples. In contrast, Ald (18:1Δ2) levels strikingly increased after TPP reduction (Fig. 3C). The relative fatty aldehydes ratio yielded an estimated hydroperoxide-to-dioxetane ratio of 96:4, closely matching the value obtained in the phospholipid analysis. Together, these data show that vinyl ether bond oxidation by O_2 ($^1\Delta_g$) predominantly proceeds by the *ene* reaction mechanism, yielding plasmalogen hydroperoxyacetal as a major primary product.

Characterization of fatty aldehydes generated from plasmalogen hydroperoxides

Previous studies have detected long-chain fatty aldehydes from plasmalogen oxidation (9, 35–38). Here, we developed an LC–HRMS method to specifically detect fatty aldehydes using the 7-(diethylamino)coumarin-3-carbohydrazide (CHH) (39) and 7-mercapto-4-methylcoumarin (CSH) probes. As mentioned above, heptadecanal [Ald (17:0)] was used as a marker for dioxetane and 2-octadecenal [Ald (18:1 Δ2)], an alpha–beta unsaturated fatty aldehyde, was used as a marker for plasmalogen hydroperoxides [pPE (p18:0-OOH/18:1)].

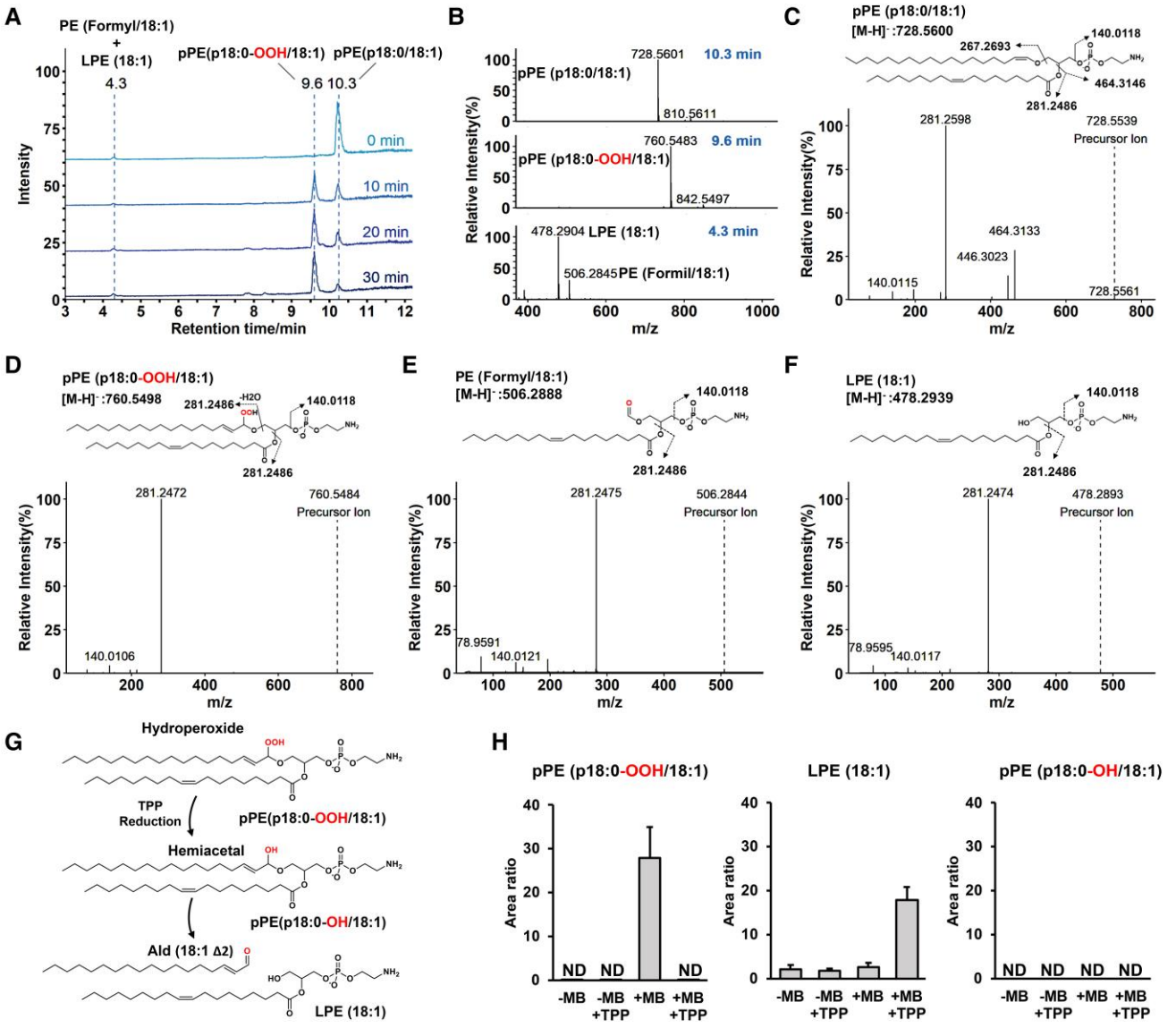

Fig. 2. Characterization of plasmalogen photooxidation products by LC–HRMS analysis. A) Total ion chromatograms of pPE (p18:0/18:1) photooxidized with MB for 0, 10, 20, and 30 min. B) MS1 mass spectra of pPE oxidation products detected at 4.3, 9.6, and 10.3 min. MS2 mass spectra of pPE (p18:0/18:1) (C), pPE(p18:0-OOH:18:1) (D), PE (formyl/18:1) (E), and LPE(18:1) (F). G) Reaction scheme illustrating the reduction of pPE (p18:0-OOH/18:1) with TPP, resulting in the formation of a hemiacetal. This hemiacetal undergoes cleavage, yielding a fatty aldehyde, Ald (18:1Δ2), and LPE (18:1). H) Relative concentrations of plasmalogen-oxidized products before and after TPP addition. Reaction conditions: 1 mM of pPE (p18:0/18:1) was photooxidized in the presence of 50 μM of MB at −40°C under the following conditions: (−MB) without methylene blue; (+MB) with methylene blue; and (+MB + TPP) with MB and with TPP. Data are shown as area ratio ± SEM.

Firstly, aldehydes derivatized with the CHH probe (Fig. 4A) were characterized by mass spectrometry. The Ald (17:0)-CHH adduct detected in the photooxidized pPE sample exhibited the same retention time and fragmentation profile as the commercial Ald (17:0) standard. Both MS/MS spectra showed a prominent fragment ion corresponding to the CHH probe at m/z 244.0968 and a fragment ion corresponding to the fatty alkyl chain at m/z 252.2702 (Fig. 4B and C). Similarly, Ald (18:1 Δ2)-CHH adduct showed a precursor ion at m/z 524.3847 and a fragment ion corresponding to the fatty alkyl chain at m/z 279.2830 (Fig. 4D).

Next, fatty aldehydes containing alpha–beta carbonyl group were derivatized with CSH, a coumarin derivative containing a thiol group, as a second probe. The derivatization method using the CHH and CSH fluorescent probes was validated using commercially available Ald (16:1 Δ2) and Ald (16:0) (Fig. S4). As illustrated for Ald (16:1 Δ2), the thiol group in the CSH probe reacts with the beta-carbon in the fatty aldehyde, preserving the aldehyde group and allowing subsequent derivatization with the CHH probe (Fig. 4E). The doubly derivatized aldehyde exhibited a fragmentation profile showing the loss of the probes and fragments indicating the presence of the alpha–beta unsaturated carbonyl group (Fig. 4F). Of note, a similar fragmentation pattern was observed for Ald (18:1 Δ2) detected in the photooxidized plasmalogen sample after TPP reduction (Fig. 4G), clearly confirming the presence of alpha–beta unsaturated carbonyl groups.

Detection of excited triplet carbonyls and singlet oxygen from oxidized plasmalogen species

Dioxetane decomposition generates excited triplet carbonyls and O_2 ($^1\Delta_g$) (40, 41). Excited triplet carbonyls have been linked to normal and deleterious effects due to their radical-like chemical and

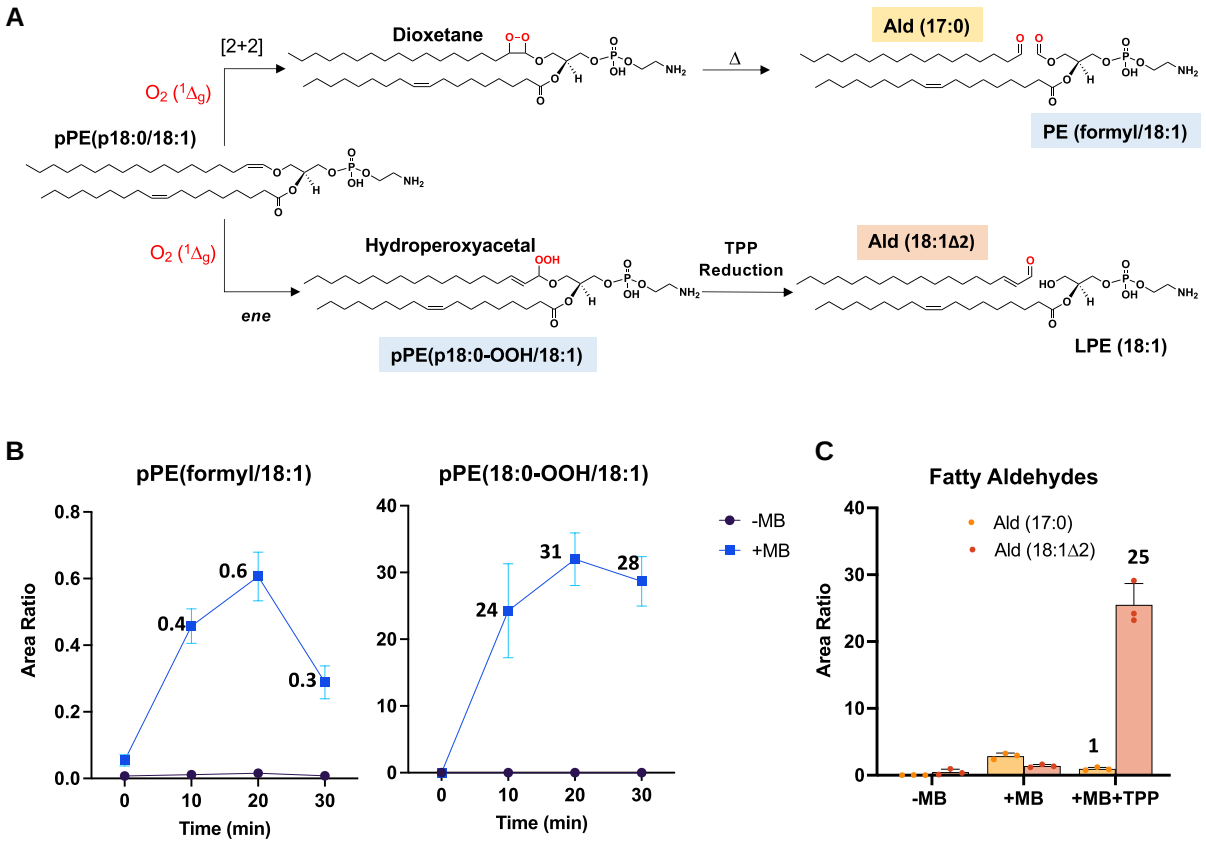

Fig. 3. Determination of the relative ratio between dioxetane and hydroperoxyacetal pathways. A) Reaction scheme illustrating the oxidation of plasmalogen vinyl ether bond by O_2 ($^1\Delta_g$). Top—the [2 + 2] cycloaddition mechanism leads to the formation of dioxetane, which undergoes subsequent cleavage to produce PE (formyl/18:1) and Ald (17:0). Bottom—The *ene* reaction generates hydroperoxyacetal, which is then reduced to produce LPE (18:1) and Ald (18:1Δ2). B) Quantification of PE (formyl/18:1) and pPE (p18:0-OOH/18:1). C) Quantification of fatty aldehydes, Ald (17:0) and Ald (18:1Δ2), after 30 min of irradiation. Reaction conditions were the same as in Figure 2. Data are shown as area ratio ± SEM.

physicochemical properties (42, 43). They often return to the ground state producing ultra-weak photon emission in the visible region (44) and participate in energy transfer reactions with other molecules, including molecular oxygen [O_2 ($^3\Sigma_g$)], producing O_2 ($^1\Delta_g$) (41) (Fig. 5A).

To demonstrate the generation of excited triplet carbonyls, plasmalogen samples photooxidized at −40°C were allowed to naturally heat up to room temperature, and visible-light emission was recorded using a photomultiplier. As expected, intense light emission was observed from the photooxidized pPE (p18:0/18:1) sample but not from PE (18:1/18:1) (Fig. 5B). The generation of excited triplet carbonyls was further confirmed by using dibromoanthracene (DBA) as a triplet carbonyl enhancer (42), which produced a noticeable enhancement in the visible-light emission (Fig. 5C).

After detecting excited triplet carbonyls, our subsequent investigation focused on the detection of O_2 ($^1\Delta_g$) generated through energy transfer from excited triplet carbonyls to molecular oxygen. O_2 ($^1\Delta_g$) detection was performed by the measurement of its monomolecular light emission in the near-infrared (NIR) region at 1,270 nm (20, 31). Notably, a light emission persisting for several minutes was observed in the photooxidized pPE (p18:0/18:1) (Fig. 5D). The production of O_2 ($^1\Delta_g$) was confirmed by chemical trapping with 9,10-diphenylanthracene (DPA). This chemical probe reacts rapidly ($k = 1.3 \times 10^6$ $M^{-1}s^{-1}$) with O_2 ($^1\Delta_g$), resulting in a stable endoperoxide ($DPAO_2$) that can be detected by HPLC (31, 45) (Fig. 5A). DPA was added after photooxidation at low temperature and incubated at room temperature for 1 h in the dark. HPLC analysis confirmed the formation of $DPAO_2$ (Fig. 5E). Together, these data confirm the production of O_2 ($^1\Delta_g$) from photooxidized plasmalogen species.

Characterization of plasmalogen hydroperoxyacetal decomposition products

Lipid hydroperoxides react with metal ions such as FeII and CeIV, producing peroxyl radicals and O_2 ($^1\Delta_g$) via the Russell mechanism (31, 46). In this mechanism, two peroxyl radicals react head to head to form a linear tetroxide intermediate that decomposes producing a ketone, an alcohol, and an O_2 ($^1\Delta_g$) (30). We have previously demonstrated that lipid hydroperoxides generate O_2 ($^1\Delta_g$) and the corresponding alcohol and ketone products through the Russell mechanism (31–33, 47). Here, our aim was to characterize the major oxidation products resulting from the metal ion-catalyzed decomposition of pPE (p18:0-OOH/18:1). Plasmalogen hydroperoxyacetal reaction with metal ions produces peroxyl radicals that produce a hemiacetal and a ketone as final products. The hemiacetal intermediate is cleaved, producing LPE (18:1) and Ald (18:1 Δ2), while the ketone group forms an ester bond at n-1 position producing a diacyl PE, (Fig. 6A). For comparison, we also studied the products formed by the reaction of PE hydroperoxides (Fig. 6B).

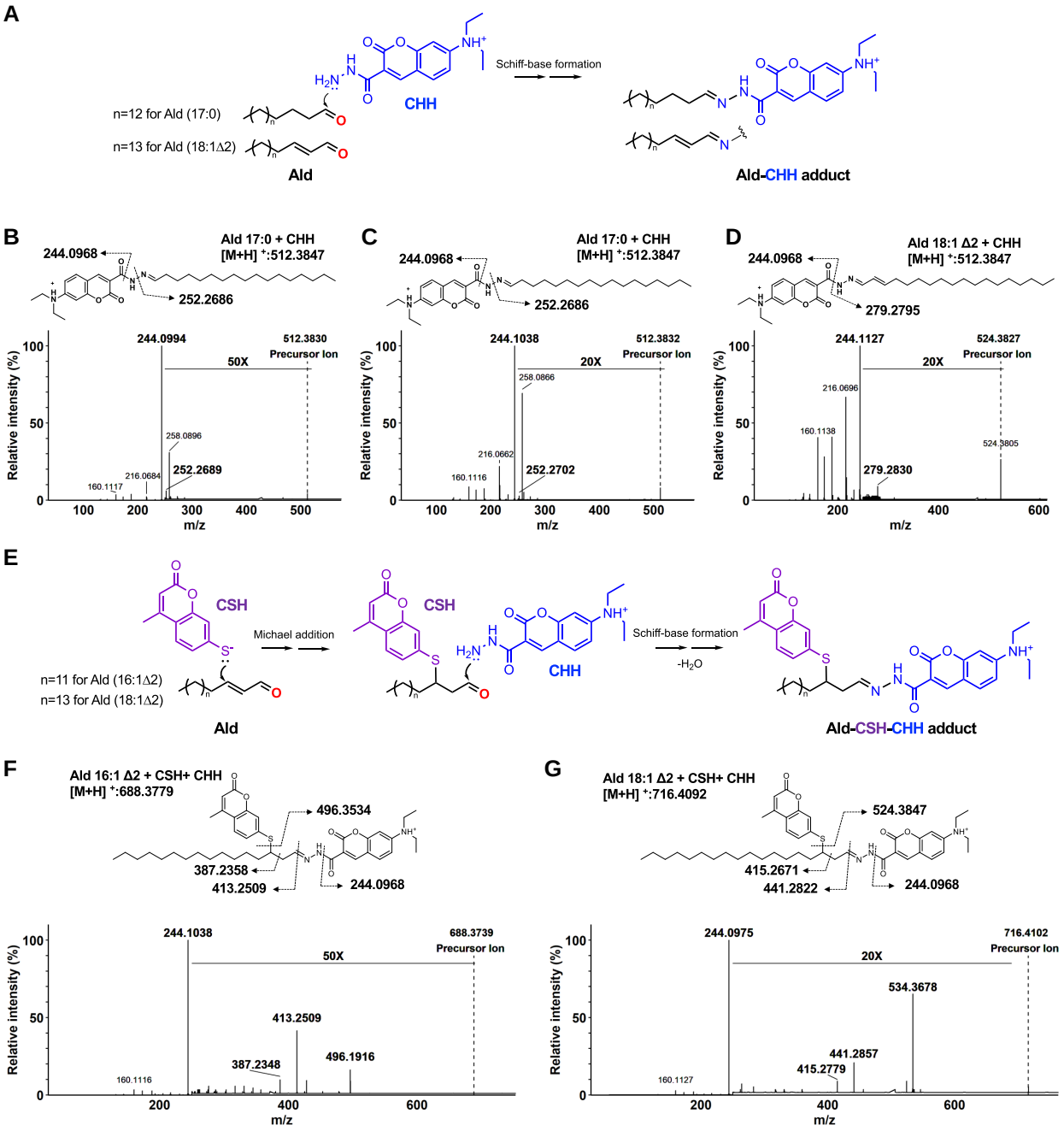

Fig. 4. Characterization of long-chain fatty aldehydes by mass spectrometry. A) Scheme illustrating fatty aldehyde (Ald) derivatization with the CHH probe. MS/MS spectra of the Ald-CHH adducts detected for: Ald (17:0) commercial standard (B), Ald (17:0) generated from pPE (p18:0/18:1) photooxidation (C), and Ald (18:1 Δ2) generated from pPE (p18:0-OOH/18:1) reduction with TPP (D). E) Scheme depicting alpha–beta unsaturated fatty aldehyde derivatization with CSH and CHH probes. MS/MS spectra of the Ald–CSH–CHH adduct detected for: Ald (16:1 Δ2) commercial standard (F) and Ald (18:1 Δ2) generated from pPE (p18:0-OOH/18:1) reduction with TPP (G).

Mass spectrometry analysis showed that plasmalogen hydroperoxyacetal is completely consumed in the presence of CeIV or FeII, producing LPE (18:1) and PE (18:1Δ2/18:1) as major products (Fig. 6C). In contrast, some PE hydroperoxide remained intact after incubation with CeIV or FeII. As expected, PE hydroperoxide decomposition generated PE species containing the corresponding alcohol and ketone groups (Fig. 6D). Together, these results show that plasmalogen hydroperoxyacetal is totally decomposed by metal ions producing LPE and an ester, the diacyl PE containing alpha–beta unsaturated carbonyl group at the sn-1 position. The diacyl PE showed the same MS/MS spectrum of PE (18:1/18:1) (Fig. S5), albeit with slightly different retention times probably due to different location of the double bond in the sn-1 acyl chain (Fig. 7A). Furthermore, we confirmed the presence of alpha–beta unsaturated carbonyl group by reacting with the CSH probe and detecting PE (18:1Δ2/18:1)-CSH adduct by mass spectrometry. The MS/MS spectra of this adduct showed the characteristic CSH fragment ion at m/z 191.0172, along with fragment ions arising from sn-1 and sn-2 acyl chain cleavages (Fig. 7B).

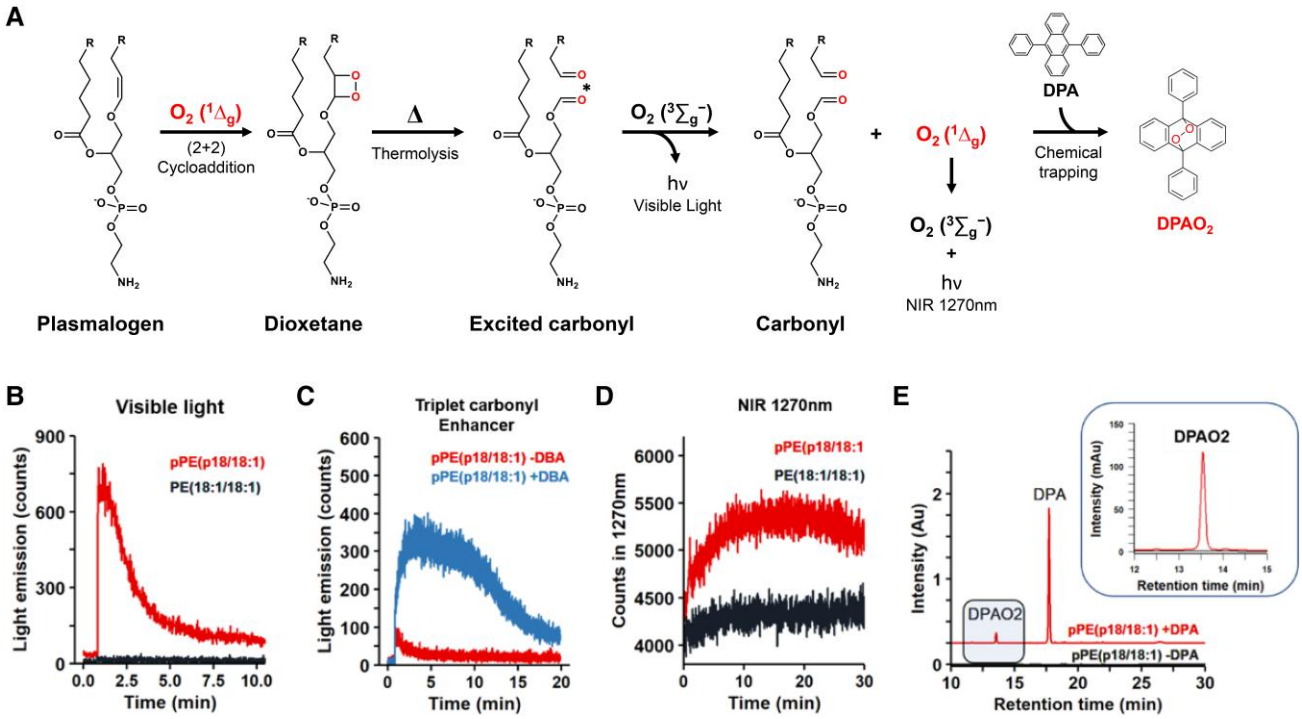

Fig. 5. Generation of excited triplet carbonyls and singlet molecular oxygen from plasmalogen dioxetane intermediate. A) Scheme illustrating the formation of dioxetane through the reaction of O_2 ($^1\Delta_g$) with the vinyl ether bond. Dioxetane thermolysis yields carbonyl species, one of them in the excited state. These excited triplet carbonyls can emit light in the visible region or transfer energy to molecular oxygen, resulting in the generation of O_2 ($^1\Delta_g$). Excited singlet molecular oxygen production was confirmed by light emission in the NIR region (1,270 nm) and chemical trapping of O_2 ($^1\Delta_g$) with DPA. B) Visible-light emission resulting from dioxetane thermolysis. C) Enhancement of triplet carbonyl light emission using 10 mM of DBA. D) NIR light emission at 1,270 nm. E) Chemical trapping of O_2 ($^1\Delta_g$) by DPA and analysis of $DPAO_2$ by HPLC (UV 210 nm). Light emission and chemical trapping experiments were performed using 1 mM of pPE (p18:0/18:1) or PE (18:1/18:1) solutions that were photooxidized with MB at −40°C for 30 min.

Characterization of singlet molecular oxygen production from plasmalogen hydroperoxyacetal

To examine the production of $O_2(^1\Delta_g)$ resulting from the reaction of plasmalogen hydroperoxyacetal with metal ions, we measured the light emission in the NIR region at 1,270 nm. An intense emission signal was observed in the reaction of pPE (p18:0-OOH/18:1) with CeIV (Fig. 8A). For comparison, we also measured the light emission generated from linoleic acid hydroperoxide (LAOOH) (Fig. 8B), a positive control that has been previously shown to be produced $O_2(^1\Delta_g)$ via the Russell mechanism (31). Interestingly, both hydroperoxides produced light emission at 1,270 nm with similar intensity and kinetics.

Furthermore, we confirmed the generation of O_2 ($^1\Delta_g$) from pPE (p18:0-OOH/18:1) by the acquisition of the NIR light emission spectrum, showing a maximum intensity at 1,270 nm (Fig. 8C). As a control, we also acquired the emission spectra for 1,4-dimethyl naphtalene endoperoxide ($DMNO_2$), a classical chemical generator of O_2 ($^1\Delta_g$) (Fig. 8D). To estimate the relative yield of $O_2(^1\Delta_g)$, we used the emission signal from $DMNO_2$ as a reference (Fig. S6). The yield of $O_2(^1\Delta_g)$ generated from plasmalogen hydroperoxide was 3.2%, consistent with previous yields of $O_2(^1\Delta_g)$ reported for lipid hydroperoxides reacting by the Russell mechanism (31). Together, these results clearly demonstrate that plasmalogen hydroperoxyacetal generates $O_2(^1\Delta_g)$ upon reaction with metal ions.

Discussion

In this study, we demonstrate that the oxidation of plasmalogens by O_2 ($^1\Delta_g$) generates reactive intermediates capable of promoting the formation of excited species and electrophilic lipid species. Chemiluminescence measurements taken in the visible and NIR regions (specifically at 1,270 nm) detected characteristic light emissions associated with the production of excited triplet carbonyls and O_2 ($^1\Delta_g$). The generation of excited triplet carbonyls from dioxetane was confirmed through light emission measurements in the visible region, as well as by observing enhanced light emission upon the addition of DBA, a triplet chemiluminescence enhancer. Moreover, our study offers compelling evidence demonstrating the production of O_2 ($^1\Delta_g$) through the reaction between plasmalogen hydroperoxyacetal and metal ions. Particularly, the intense light emission signal detected in the NIR region, showing an emission peak at 1,270 nm, serves as unequivocal evidence for O_2 ($^1\Delta_g$) generation.

In terms of mechanism, the generation of excited triplet carbonyls and O_2 ($^1\Delta_g$) from plasmalogen oxidation can be explained by two pathways as depicted in Figure 1. Firstly, the [2 + 2] cycloaddition results in the formation of an unstable 1,2-dioxetane intermediate, which then undergoes thermolysis to produce excited triplet carbonyls (Fig. 1A). Secondly, the *ene* reaction leads to the formation of plasmalogen hydroperoxyacetal. This compound subsequently generates O_2 ($^1\Delta_g$) through reactions involving the combination of peroxyl radicals via the Russell mechanism (Fig. 1B).

The relative proportion between these two pathways was carefully examined using mass spectrometry analysis of phospholipid oxidation products. Our data reveal that plasmalogen predominantly reacts with O_2 ($^1\Delta_g$) through the *ene* reaction, yielding plasmalogen hydroperoxyacetal as the major product (98%), while the formyl PE resulting from dioxetane cleavage was detected at minimal quantities (2%). This finding was further supported by

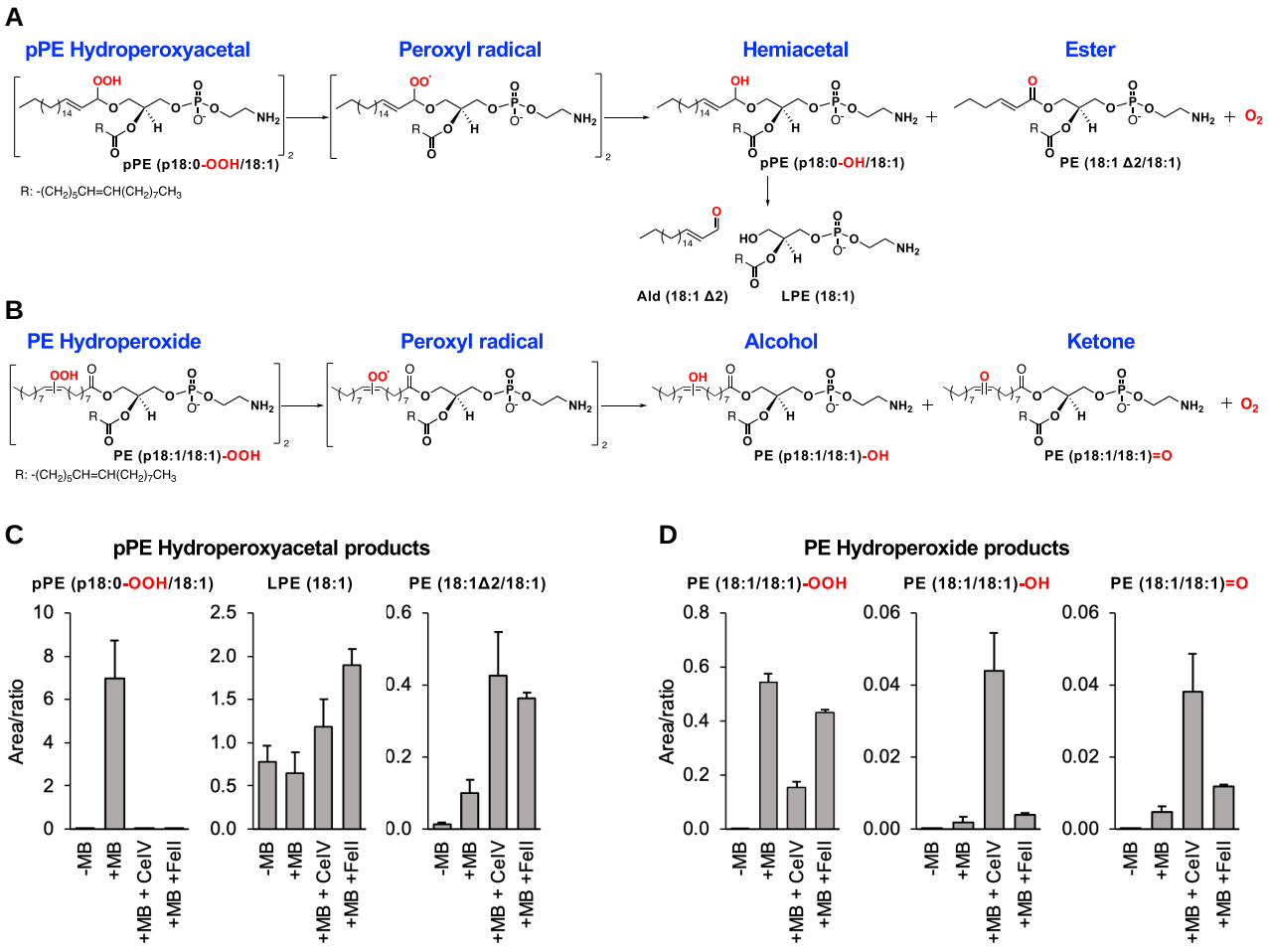

Fig. 6. Plasmalogen hydroperoxyacetal reacts with metal ions, producing alpha–beta unsaturated fatty aldehydes and LPE. A and B) Scheme depicting the reaction products for pPE hydroperoxyacetal and PE hydroperoxides. C and D) Quantification of phospholipid oxidation products by LC–HRMS. Reaction conditions: 1 mM of plasmalogen solution photooxidized with MB at −40°C for 30 min was mixed with 50 μM of CeIV or FeII in $CHCl_3$/methanol/water (90:9:1 v/v/v) for 1 h.

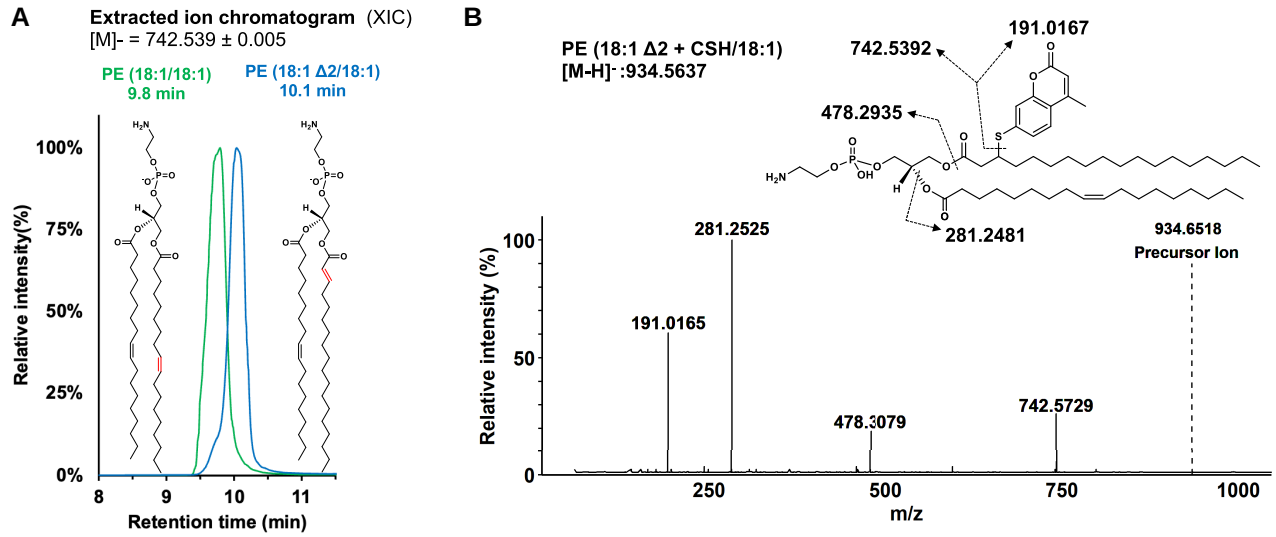

Fig. 7. Characterization of alpha–beta unsaturated carbonyl group in PE (18:1Δ2/18:1). A) Extracted ion chromatogram of m/z 742.539 in photooxidized pPE (p18:0/18:1) treated with CeIV (peak at 9.8 min) and the commercial PE(18:1/18:1) standard (peak at 10.1 min). B) MS/MS spectrum of PE (18:1Δ2/18:1)-CSH adduct.

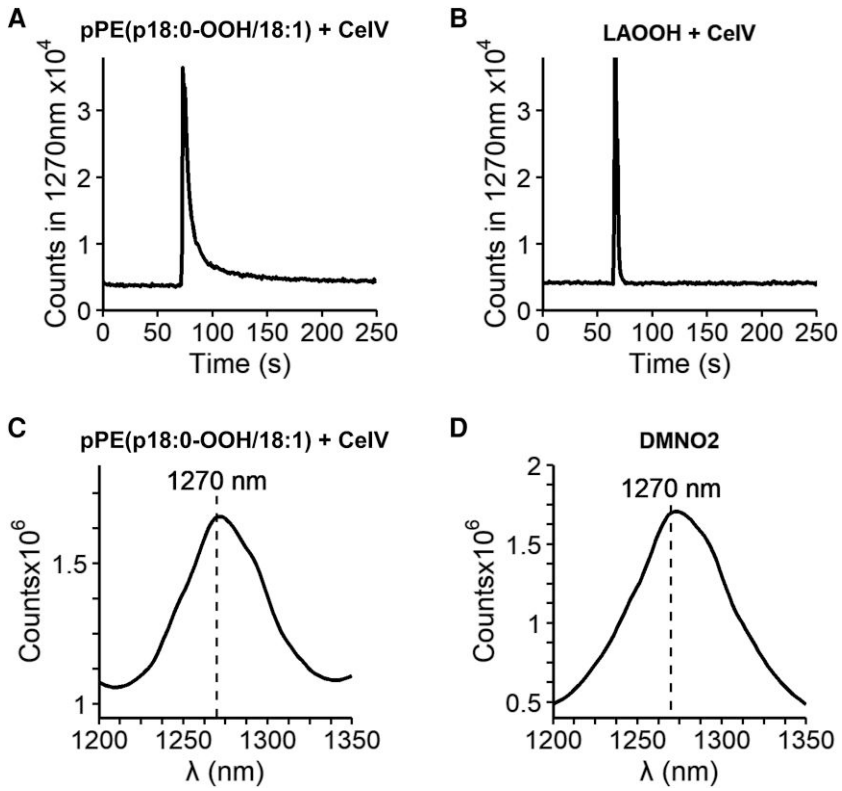

Fig. 8. Singlet molecular oxygen generation from plasmalogen hydroperoxyacetal reaction with CeIV. A) Light emission signal at 1,270 nm obtained for the reaction of 5 μM of pPE (p18:0-OOH/18:1). B) Comparison with the reaction using LAOOH. C) NIR light emission spectrum obtained in the reaction of 100 μM of pPE (p18:0-OOH/18:1) with 75 μM of CeIV. D) NIR light emission spectrum obtained during the thermolysis of 1 mM of $DMNO_2$.

the analysis of relative yields of fatty aldehydes derived from dioxetane and hydroperoxide intermediates. We employed an LC–MS method specifically developed to detect fatty aldehydes containing alpha–beta unsaturated carbonyl groups. Notably, Ald (18:1 Δ2), the alpha–beta unsaturated fatty aldehyde derived from plasmalogen PE (p18:0-OOH/18:1), significantly increased after reduction with TPP, becoming the most abundant aldehyde (96%) detected in the reaction. In contrast, heptadecanal (Ald 17:0), a product formed by dioxetane cleavage, was detected at minor levels (4%). Thus, we confirmed using two different LC–HRMS methods that plasmalogen photooxidation predominantly generates hydroperoxyacetal as the major primary photooxidation product.

Earlier research has reported the detection of plasmalogen hydroperoxyacetal, which forms at the vinyl ether bond of plasmalogen species through photosensitized and radical oxidations (9, 12, 23). Although the biological fate of these hydroperoxides remains unknown, it is well established that phospholipid hydroperoxides are rapidly reduced to hydroxides by antioxidant enzymes, such as GPx4. Phospholipid hydroperoxides can react with metal ions, producing alkoxyl and peroxyl radicals. These radicals undergo intra- and inter-molecular reactions, producing aldehydes and truncated species, which can cause membrane rupture (48) and cell death by ferroptosis (49). Moreover, phospholipid hydroperoxides generate O_2 ($^1\Delta_g$) upon reacting with metal ions (31), heme proteins (33), and other oxidants such as hypochlorous acid (32). Notably, here we also demonstrate that plasmalogen hydroperoxyacetal reacts with metal ions (FeII and CeIV) producing O_2 ($^1\Delta_g$) through the Russell mechanism. This mechanism is supported by the detection of the corresponding alcohol and ketone products (Fig. 1B). In the case of pPE (p18:0-OOH/18:1), the conversion of hydroperoxyacetal to an alcohol yields a hemiacetal that cleaves, generating LPE and alpha–beta unsaturated fatty aldehyde. Interestingly, the conversion of hydroperoxyacetal to a ketone generates an ester-bonded acyl chain containing an alpha–beta unsaturated carbonyl group. The reactivity and biological consequences of this electrophilic phospholipid species deserve further investigation.

Collectively, the results presented herein demonstrate that plasmalogen oxidation generates reactive intermediates with potential prooxidant and deleterious roles. These intermediates include triplet carbonyls, O_2 ($^1\Delta_g$), alpha–beta unsaturated phospholipids, and fatty aldehydes. Notably, excited molecules can propagate oxidative reaction in the absence of light, a phenomenon known as "dark photochemistry" (27, 42). Additionally, triplet carbonyls can cause deleterious effects in cells by transferring energy to other biomolecules, a process recently described for excited melanin, neurotransmitters, and hormones, leading to the formation of carcinogenic DNA modifications (26, 50). Hence, excited triplet carbonyl species emerges as a product of plasmalogen oxidation with deleterious action. Furthermore, alpha–beta unsaturated lipids have the capacity to modify peptides, proteins, and other biomolecules. These aldehydes are susceptible to Michael addition reactions in the presence of nucleophiles, such as the sulfhydryl group of cysteines (51). For instance, 2-hexadecenal, an alpha–beta unsaturated long-chain aldehyde produced in sphingolipid enzymatic and nonenzymatic metabolism (52), has been reported to induce cytoskeletal reorganization and apoptosis in various cell types (53–55).

While typically regarded as antioxidants, our data show that plasmalogens act as prooxidants when the vinyl ether double bond reacts with singlet molecular oxygen. This finding holds particular significance for understanding the biological roles of O_2

($^1\Delta_g$) and stress responses in tissues and microorganisms exposed to sunlight (56), extending beyond the direct effects observed from UV radiation. This includes the dark reactions occurring post-light exposure in the skin, leading to DNA photoproducts long after UV exposure (26, 27) and the effects of other wavelength ranges, such as visible light acting on endogenous sensitizers (57). Overall, our study highlights potential prooxidant pathways of plasmalogens, revealing their involvement in excited species generation and reactive lipid production, thus contributing to a deeper understanding of oxidative processes in biological systems.

Materials and methods

Materials

The complete list of materials and suppliers is provided in the supplementary information.

Plasmalogen photooxidation

pPE(p18:0/18:1) was photooxidized at a concentration of 1 mM in the presence of 0.3 mM of methylene blue (MB) in $CHCl_3$ (or $CDCl_3$ for luminescence emission). PE (14:0/14:0) 0.1 mM was used as an internal standard. Samples were photooxidized with an LED lamp (632 nm, 41 ± 1 Wm^{-2}) for 30 min in a −40°C bath (dry ice and acetonitrile) while bubbling oxygen. Aliquots were collected for 10, 20, and 30 min and then diluted 100 times before LC–HRMS analysis. For comparison, a pPE mixture purified from bovine brain (approximately 5 mM) was photooxidized in the presence of MB in $CHCl_3$ under the same conditions.

Lipidomic analysis

Plasmalogen oxidation was comprehensively analyzed using lipidomic analysis conducted on an electrospray ionization quadrupole time-of-flight (ESI-QTOF) mass spectrometer (Triple TOF 6600, Sciex, Concord, USA) coupled with ultra-high-performance liquid chromatography (UHPLC Nexera, Shimadzu, Kyoto, Japan). The samples were loaded into a C18 column (CORTECS UPLC C18 column, 1.6 µm, 2.1 mm i.d. × 100 mm) with a flow rate of 0.2 mL min^{-1} and an oven temperature maintained at 35°C. For reverse-phase LC, mobile phase A consisted of water/acetonitrile (60:40, v/v), while mobile phase B composed of isopropanol/acetonitrile/water (88:10:2, v/v/v). Mobile phases A and B contained formic acid at a final concentration of 10 mM. Lipids were separated by a 20-min linear gradient as follows: from 40 to 100% B over the first 10 min, hold at 100% B from 10 to 12 min, decreased from 100 to 40% B during 12–13 min, and hold at 40% B from 13 to 20 min. The mass spectrometer was operated in the negative ionization mode with the ion spray voltage at −4.5 V and the cone voltage at −80 V. Additional parameters included curtain gas set at 25 psi, nebulizer and heater gases at 45 psi, and interface heater of 450°C. MS1 and MS2 were acquired by information-dependent acquisition using the following parameters: m/z scan range 200–2,000 Da; cycle time period of 1.05 s with 100 ms acquisition time for MS1 scan; and 25 ms acquisition time to obtain the top 36 precursor ions. The LC–HRMS data were acquired by Analyst 1.7.1, and the data were analyzed with PeakView. Lipid molecular species were manually identified based on their exact masses, specific fragments, and/or neutral losses. A maximum error of 5 mDa was defined for the attribution of the precursor ion. After identification, the area of lipid species was obtained by MS1 data using MultiQuant. Each peak integration was carefully inspected for correct peak detection and accurate area determination. PE(14:0/14:0) was used as an internal standard for pPE data normalization.

Quantification of plasmalogen hydroperoxides

For the quantification of plasmalogen hydroperoxides, the method based on triphenylphosphine (TPP) reaction with hydroperoxides was employed (58). Briefly, 25 µL of the photooxidized pPE solution was added to a 100-µL insert. The solvent was removed using a nitrogen stream, and 50 µL of 5 mM TPP in acetonitrile was added. The mixture was incubated for 30 min in the dark at room temperature under stirring at 300 rpm. Subsequently, TPP and its oxide (TPPO) were analyzed by UHPLC (Nexera, Shimadzu, Kyoto, Japan) using a C8 column (CORTECS UPLC, 1.6 µm, 2.1 mm i.d. × 100 mm) with a flow rate of 0.3 mL/min and an oven temperature maintained at 40°C. The injection volume was 5 µL, and the UV detection wavelength was 220 nm. UHPLC separation was performed with water (solvent A) and acetonitrile (solvent B) using the following steps: a linear gradient from 40 to 100% B over 0–1 min, holding at 100% B from 1 to 2 min, decreasing from 100 to 40% B during 2–2.1 min, and holding at 40% B from 2.1 to 4.5 min. A calibration curve was constructed with tert-butyl hydroperoxide or linoleic acid hydroperoxide (LAOOH).

Plasmalogen hydroperoxide incubation with metal ions

Incubations of plasmalogen hydroperoxides with metal ions were performed by mixing 5 µM of pPE(p18:0-OOH/18:1) or PE (18:1/18:1)-OOH with CeIV or FeII in $CHCl_3$/methanol/water (90:9:1 v/v/v) at 37°C for 1 h. Reaction products were analyzed by LC–HRMS using PE (14:0/14:0) at 0.5 µM as an internal standard. The LC system setup included a valve that was used to discard the initial 5 min to avoid interference from metal ions (CeIV or FeII) in the mass spectrometry data acquisition. For singlet oxygen light emission measurement in the NIR region, we added 308 µL of pPE(p18:0-OOH/18:1) or LAOOH in $CDCl_3$ in a cuvette. Then, 92 µL of a MeOD/D_2O (914:6 v/v) solution containing metal ions (CeIV or FeII) was infused into the solution within 60 s under stirring, resulting in a final solution with 5 µM of hydroperoxide and 75 µM of metal ion (CeIV or FeII).

Fatty aldehyde derivatization

For the analysis of alpha–beta unsaturated lipids, 100 µM of photooxidized pPE with or without FeII/CeIV was incubated with 5 mM of CSH in acetonitrile with 0.1% triethylamine for 2 h at room temperature before incubation with CHH. Derivatized fatty aldehyde samples were analyzed by UHPLC (Nexera, Shimadzu, Kyoto, Japan). Aliquots of 5 µL of the sample were injected into a reversed-phase C8 column (100 × 2.1 mm, 1.6 µm particle size) with a flow rate of 0.2 mL min^{-1}, an oven temperature maintained at 35°C, and an RF-10Axl fluorescence detector. The HPLC mobile phase consisted of water with 0.1% formic acid (solvent A) and methanol with 0.1% formic acid (solvent B), and the flow rate was 0.3 mL/min. The fluorescent adducts were separated using the following conditions: 60% B for 2 min, 60–100% B for 9 min, 92% B for 3 min, 100–60% B for 1 min, and 60% B for 3 min. The excitation and emission wavelengths were fixed at 450 and 468 nm, respectively.

Fatty aldehyde analysis by mass spectrometry

The aldehydes derivatized with CHH were analyzed by LC–HRMS (Triple TOF 6600, Sciex, Concord, USA) interfaced with UHPLC (Nexera, Shimadzu, Kyoto, Japan). The chromatographic

conditions were the same as for the fluorescence analysis. To avoid ion suppression due to excess CHH probe, we used a valve to discard the first initial 5 min (Fig. S6E) in the LC–HRMS analysis. All aldehydes entering the MS were analyzed in the positive mode (Fig. S6F). The final derivation conditions were 50 μM of aldehydes or 50 μM of pPE and 1 mM of CHH in isopropanol with 0.1% formic acid.

Excited triplet carbonyl light emission measurements in the visible region

All reactions were carried out in a quartz tube under constant stirring at room temperature (final volume = 600 μL). The light emission in the visible region was immediately recorded by a FLSP 920 photon counter (Edinburgh Instruments, Edinburgh, UK) with a PMT Hamamatsu detector R9110 maintained at −20°C by a PMT cooler CO1 (Edinburgh Instruments). 1 mM of pPE (p18:0/18:1) or PE (18:1/18:1) photooxidized at −40°C in $CDCl_3$ was added to a cuvette and naturally warmed to room temperature. For excited triplet carbonyl enhancer experiments, 9,10-dibromoanthracene (DBA) was added before the reading at a final concentration of 10 mM. For chemical trapping, 9,10-diphenylanthracene (DPA) was added prior to the reading at a final concentration of 10 mM, incubated for 1 h at room temperature, and then analyzed by HPLC at 210 nm (31).

Singlet molecular oxygen light emission measurements in the NIR region

The monomolecular light emission of O_2 ($^1\Delta_g$) was measured using two photocounting apparatus developed in our lab, equipped with a monochromator capable of selecting emissions in the NIR region (950–1,400 nm). The NIR spectra were recorded by a FLSP 920 photon counter (Edinburgh Instruments, Edinburgh, UK) consisting of a H10330A-45 NIR-PMT detector (Hamamatsu, Japan) that is coupled to a thermoelectric cooler module apparatus maintained at −60°C to reduce the dark current. The power was provided by a high-voltage DC power supply, and the applied potential was set to −0.8 kV. The light emitted from the sample was processed through a monochromator (TMS/DTMS300, Edinburgh Analytical Instruments, UK) equipped with a diffraction grating capable of selecting wavelengths in the infrared region. The phototube output was connected to the computer, and the signal was acquired. The monochromator was controlled, and the data were acquired using the F-900 version 6.22 software (Edinburgh Analytical Instruments, Livingston, UK). The NIR light emission kinetics at 1,270 nm was performed in a second photocounting apparatus using a band pass filter placed between the cuvette and the photomultiplier. All sample components were mixed and poured into a glass cuvette (35 × 7 × 55 mm) maintained at 25°C.

Acknowledgments

The authors thank Adriano Britto Chaves-Filho and Marcos Y. Yoshinaga for their support with mass spectrometry and lipidomic analysis, Miyamoto Lab members and Cepid-Redoxoma group for their constant support and discussions, and Erick L. Bastos and Etelvino Bechara for helpful discussions.

This manuscript was posted on a preprint: https://doi.org/10.1101/2024.02.22.581635

Supplementary Material

Supplementary material is available at *PNAS Nexus* online.

Funding

This study was supported by the Fundação de Amparo à Pesquisa do Estado de São Paulo (FAPESP, CEPID-Redoxoma, 13/07937-8), Conselho Nacional de Desenvolvimento Científico e Tecnológico (CNPq 313926/2021-2 to S.M., 304350/2023-0 to P.D.M.), Coordenação de Aperfeiçoamento de Pessoal de Nível Superior (CAPES, Finance Code 001), and Pro-Reitoria de Pesquisa da Universidade de São Paulo (PRPUSP). The PhD scholarship of R.L.F. was supported by FAPESP [17/16140-7].

Author Contributions

R.L.F. and S.M. designed the research; R.L.F., F.M.P., H.C.J., K.C.F., and L.R.D. performed the research; R.L.F., F.M.P., L.R.D., M.S.B., P.D.M., and S.M. analyzed the data; and R.L.F., M.S.B., P.D.M., and S.M. wrote the paper.

Data Availability

Raw mass spectrometry analysis files (wiff data) are available at MassIVE (doi:10.25345/C56Q1ST9M) with the identifier MSV000094760.

References

1 Nagan N, Zoeller RA. 2001. Plasmalogens: biosynthesis and functions. *Prog Lipid Res*. 40:199–229.
2 Wallner S, Schmitz G. 2011. Plasmalogens the neglected regulatory and scavenging lipid species. *Chem Phys Lipids*. 164:573–589.
3 Braverman NE, Moser AB. 2012. Functions of plasmalogen lipids in health and disease. *Biochim Biophys Acta*. 1822:1442–1452.
4 Jiménez-Rojo N, Riezman H. 2019. On the road to unraveling the molecular functions of ether lipids. *FEBS Lett*. 593:2378–2389.
5 Goldfine H. 2010. The appearance, disappearance and reappearance of plasmalogens in evolution. *Prog Lipid Res*. 49:493–498.
6 Dean JM, Lodhi IJ. 2017. Structural and functional roles of ether lipids. *Protein Cell*. 9:196–206.
7 Heymans HS, Schutgens RB, Tan R, van den Bosch H, Borst P. 1983. Severe plasmalogen deficiency in tissues of infants without peroxisomes (Zellweger syndrome). *Nature*. 306:69–70.
8 Brites P, Waterham HR, Wanders RJA. 2004. Functions and biosynthesis of plasmalogens in health and disease. *Biochim Biophys Acta*. 1636:219–231.
9 Morand OH, Zoeller RA, Raetz CR. 1988. Disappearance of plasmalogens from membranes of animal cells subjected to photosensitized oxidation. *J Biol Chem*. 263:11597–11606.
10 Zoeller RA, *et al*. 1999. Plasmalogens as endogenous antioxidants: somatic cell mutants reveal the importance of the vinyl ether. *Biochem J*. 338(Pt 3):769–776.
11 Zoeller RA, *et al*. 2002. Increasing plasmalogen levels protects human endothelial cells during hypoxia. *Am J Physiol Heart Circ Physiol*. 283:H671–H679.
12 Thompson DH, Inerowicz HD, Grove J, Sarna T. 2003. Structural characterization of plasmenylcholine photooxidation products. *Photochem Photobiol*. 78:323–330.
13 Engelmann B. 2004. Plasmalogens: targets for oxidants and major lipophilic antioxidants. *Biochem Soc Trans*. 32:147–150.
14 Aldrovandi M, Conrad M. 2020. Ferroptosis: the good, the bad and the ugly. *Cell Res*. 30:1061–1062.
15 Zou Y, *et al*. 2020. Plasticity of ether lipids promotes ferroptosis susceptibility and evasion. *Nature*. 585:603–608.

16 Cui W, Liu D, Gu W, Chu B. 2021. Peroxisome-driven ether-linked phospholipids biosynthesis is essential for ferroptosis. *Cell Death Differ*. 28:2536–2551.
17 Reed A, Ware T, Li H, Fernando Bazan J, Cravatt BF. 2023. TMEM164 is an acyltransferase that forms ferroptotic C20:4 ether phospholipids. *Nat Chem Biol*. 19:378–388.
18 Stanley CP, *et al.* 2019. Singlet molecular oxygen regulates vascular tone and blood pressure in inflammation. *Nature*. 566:548–552.
19 Maisch T, *et al.* 2007. The role of singlet oxygen and oxygen concentration in photodynamic inactivation of bacteria. *Proc Natl Acad Sci U S A*. 104:7223–7228.
20 Di Mascio P, *et al.* 2019. Singlet molecular oxygen reactions with nucleic acids, lipids, and proteins. *Chem Rev*. 119:2043–2086.
21 Ogilby PR. 2010. Singlet oxygen: there is indeed something new under the sun. *Chem Soc Rev*. 39:3181–3209.
22 Broniec A, *et al.* 2011. Interactions of plasmalogens and their diacyl analogs with singlet oxygen in selected model systems. *Free Radic Biol Med*. 50:892–898.
23 Khaselev N, Murphy RC. 2000. Structural characterization of oxidized phospholipid products derived from arachidonate-containing plasmenyl glycerophosphocholine. *J Lipid Res*. 41:564–572.
24 Cilento G, Adam W. 1988. Photochemistry and photobiology without light. *Photochem Photobiol*. 48:361–368.
25 Martinez GR, *et al.* 2004. Energy transfer between singlet (1Delta(g)) and triplet (3Sigma(g)-) molecular oxygen in aqueous solution. *J Am Chem Soc*. 126:3056–3057.
26 Premi S, *et al.* 2015. Chemiexcitation of melanin derivatives induces DNA photoproducts long after UV exposure. *Science*. 347: 842–847.
27 Brash DE, Goncalves LCP, Bechara EJH, Excited-State Medicine Working Group. 2018. Excited-state medicine working, chemiexcitation and its implications for disease. *Trends Mol Med*. 24: 527–541.
28 Brash DE, Goncalves LCP. 2023. Chemiexcitation: mammalian photochemistry in the dark. *Photochem Photobiol*. 99:251–276.
29 Girotti AW. 1998. Lipid hydroperoxide generation, turnover, and effector action in biological systems. *J Lipid Res*. 39:1529–1542.
30 Russell GA. 1957. Deuterium-isotope effects in the autoxidation of aralkyl hydrocarbons—mechanism of the interaction of peroxy radicals. *J Am Chem Soc*. 79:3871–3877.
31 Miyamoto S, Martinez GR, Medeiros MH, Mascio PD. 2003. Singlet molecular oxygen generated from lipid hydroperoxides by the Russell mechanism: studies using 18(O)-labeled linoleic acid hydroperoxide and monomol light emission measurements. *J Am Chem Soc*. 125:6172–6179.
32 Miyamoto S, *et al.* 2006. Linoleic acid hydroperoxide reacts with hypochlorous acid, generating peroxyl radical intermediates and singlet molecular oxygen. *Proc Natl Acad Sci U S A*. 103: 293–298.
33 Miyamoto S, *et al.* 2012. Cytochrome c-promoted cardiolipin oxidation generates singlet molecular oxygen. *Photochem Photobiol Sci*. 11:1536–1546.
34 Chiemezie C, Greer A. 2019. Secondary dark reactions following photodynamic treatment are more damaging than previously thought. *Photochem Photobiol*. 95:460–461.
35 Murphy MP, *et al.* 2011. Unraveling the biological roles of reactive oxygen species. *Cell Metab*. 13:361–366.
36 Felde R, Spiteller G. 1995. Plasmalogen oxidation in human serum lipoproteins. *Chem Phys Lipids*. 76:259–267.
37 Stadelmann-Ingrand S, Favreliere S, Fauconneau B, Mauco G, Tallineau C. 2001. Plasmalogen degradation by oxidative stress: production and disappearance of specific fatty aldehydes and fatty alpha-hydroxyaldehydes. *Free Radic Biol Med*. 31:1263–1271.
38 Jenkins CM, *et al.* 2018. Cytochrome c is an oxidative stress-activated plasmalogenase that cleaves plasmenylcholine and plasmenylethanolamine at the sn-1 vinyl ether linkage. *J Biol Chem*. 293:8693–8709.
39 Milic I, Hoffmann R, Fedorova M. 2013. Simultaneous detection of low and high molecular weight carbonylated compounds derived from lipid peroxidation by electrospray ionization-tandem mass spectrometry. *Anal Chem*. 85:156–162.
40 Di Mascio P, Catalani LH, Bechara EJ. 1992. Are dioxetanes chemiluminescent intermediates in lipoperoxidation? *Free Radic Biol Med*. 12:471–478.
41 Mano CM, *et al.* 2014. Excited singlet molecular O(2)((1)Deltag) is generated enzymatically from excited carbonyls in the dark. *Sci Rep*. 4:5938.
42 Ramos LD, Gomes TMV, Stevani CV, Bechara EJH. 2023. Mining reactive triplet carbonyls in biological systems. *J Photochem Photobiol B*. 243:112712.
43 Vacher M, *et al.* 2018. Chemi- and bioluminescence of cyclic peroxides. *Chem Rev*. 118:6927–6974.
44 Pospisil P, Prasad A, Rac M. 2014. Role of reactive oxygen species in ultra-weak photon emission in biological systems. *J Photochem Photobiol B*. 139:11–23.
45 Steinbeck MJ, Khan AU, Karnovsky MJ. 1992. Intracellular singlet oxygen generation by phagocytosing neutrophils in response to particles coated with a chemical trap. *J Biol Chem*. 267:13425–13433.
46 Howard J, Ingold K. 1968. Self-reaction of sec-butylperoxy radicals. Confirmation of the Russell mechanism. *J Am Chem Soc*. 90:1056–1058.
47 Uemi M, *et al.* 2011. Cholesterol hydroperoxides generate singlet molecular oxygen O-2 ((1)Delta(g)) : near-IR emission, O-18-labeled hydroperoxides, and mass spectrometry. *Chem Res Toxicol*. 24:887–895.
48 Bacellar IOL, *et al.* 2018. Photosensitized membrane permeabilization requires contact-dependent reactions between photosensitizer and lipids. *J Am Chem Soc*. 140:9606–9615.
49 Dixon SJ, *et al.* 2012. Ferroptosis: an iron-dependent form of nonapoptotic cell death. *Cell*. 149:1060–1072.
50 Goncalves LCP, *et al.* 2023. Chemiexcited neurotransmitters and hormones create DNA photoproducts in the dark. *ACS Chem Biol*. 18:484–493.
51 Higdon A, Diers AR, Oh JY, Landar A, Darley-Usmar VM. 2012. Cell signalling by reactive lipid species: new concepts and molecular mechanisms. *Biochem J*. 442:453–464.
52 Semenkova GN, *et al.* 2023. 2-Hexadecenal regulates ROS production and induces apoptosis in polymorphonuclear leucocytes. *Cell Biochem Biophys*. 81:77–86.
53 Kumar A, Byun HS, Bittman R, Saba JD. 2011. The sphingolipid degradation product trans-2-hexadecenal induces cytoskeletal reorganization and apoptosis in a JNK-dependent manner. *Cell Signal*. 23:1144–1152.
54 Schumacher F, *et al.* 2017. The sphingosine 1-phosphate breakdown product, (2E)-hexadecenal, forms protein adducts and glutathione conjugates in vitro. *J Lipid Res*. 58:1648–1660.
55 Cohen DT, Wales TE, McHenry MW, Engen JR, Walensky LD. 2020. Site-dependent cysteine lipidation potentiates the activation of proapoptotic BAX. *Cell Rep*. 30:3229–3239.e3226.
56 Gallego-García A, *et al.* 2019. A bacterial light response reveals an orphan desaturase for human plasmalogen synthesis. *Science*. 366:128.
57 Bastos EL, Quina FH, Baptista MS. 2023. Endogenous photosensitizers in human skin. *Chem Rev*. 123:9720–9785.
58 Akasaka K, Ohrui H. 2000. Development of phosphine reagents for the high-performance liquid chromatographic-fluorometric determination of lipid hydroperoxides. *J Chromatogr A*. 881: 159–170.